POLITECNICO DI TORINO
Repository ISTITUZIONALE

Torque Vectoring in Hybrid Vehicles with In-Wheel Electric Motors: Comparing SMC and PID control

(Article begins on next page)

29 June 2024

Torque Vectoring in Hybrid Vehicles with In-Wheel Electric Motors: Comparing SMC and PID control

Henrique de Carvalho Pinheiro
Politecnico di Torino
Torino, Italy
henrique.decarvalho@polito.it
ORCID: 0000-0001-8116-336X

Elisabetta Punta
CNR-IEIIT
Torino, Italy
elisabetta.punta@cnr.it
ORCID: 0000-0002-9882-3560

Massimiliana Carello
Politecnico di Torino
Torino, Italy
massimiliana.carello@polito.it
ORCID: 0000-0003-2322-0340

Alessandro Ferraris
Beond Srl
Torino, Italy
alessandro.ferraris@beond.net
ORCID: 0000-0003-0712-3399

Andrea Giancarlo Airale
Beond Srl
Torino, Italy
andrea.airale@beond.net
ORCID: 0000-0002-6857-1008

Abstract—**Electrification is a main trend in the automotive industry and in-wheel electric motors are among the underdeveloped yet promising technologies. The presence of multiple independent traction sources permits the implementation of innovative active systems and control strategies. This paper explores the possibility of a torque vectoring system applied to a FWD hybrid electric compact vehicle with two in-wheel electric motors in the rear axle and a thermal engine in the front axle. A 14 degrees of freedom co-simulation model of the vehicle is presented, developed to reproduce faithfully the non-linearities of the vehicle dynamics phenomena. Two control strategies are compared: a PID controller and a Sliding Mode Control architecture. Both achieve promising results in terms of lateral dynamics when compared to the baseline hybrid version, however the first order SMC chattering induces undesirable vibrations that undermine its potential when the vehicle is close to limit adherence condition. The effects of delays and hysteresis bands are analyzed and discussed as well as future developments of the research.**

Keywords—Vehicle Dynamics; Direct Yaw Control; Hybrid Electric Vehicles; In-Wheel Motors; Sliding Mode Control; PID, SMC control

I. INTRODUCTION

Electrification is among the main trends in the automotive industry and figures among academic studies for several years. Apart from the core goal of reducing emissions and improving overall energy efficiency [1], [2], the inclusion of Electric Machines (EM) in the powertrain architecture revels some interesting opportunities. Differently from Internal Combustion Engines (ICE) - where the usage of multiple traction sources can be quite cumbersome - with EM this opportunity is much more suitable, specially when in-wheel motors are considered. Placing the torque sources inside the wheels is not yet an industry standard, due to technology maturity, however its presence is well discussed in literature [3], [4]. The possibility to independently control the torque applied to each wheel creates the perfect conditions to the development of Direct Yaw Control (DYC) strategies, such as Torque Vectoring (TV).

The main goal of TV is to improve stability and lateral performance by applying unbalanced torque to the wheels and therefore generating a resultant yaw moment. This objective can be achieved with active differentials, active rear steering, braking action, or directly connected motors.

In terms of dynamic response, the dynamic's improvement can be translated in the following goals [4]:

- Increase vehicle's maximum lateral acceleration.
- Extend the linear response region of the steering system.
- Improve responsiveness of the steering system.

To better grasp the concepts, a plot of lateral acceleration (a_y) versus steering angle input (δ) is depicted in Fig. 1.
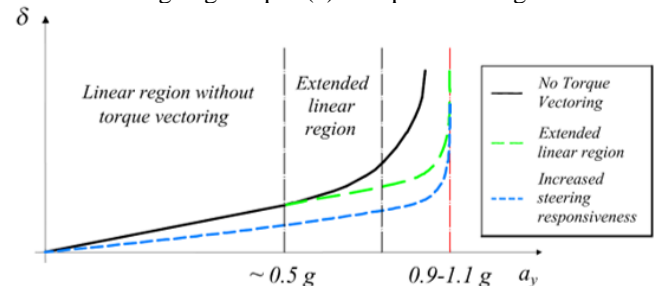

Fig. 1 - Lateral dynamics goals of TV systems.

In terms of control strategies, many different options are suitable to the application. Ranging from Proportional Integrative and Derivative (PID) controllers [4]–[7] to Model Predictive Control (MPC) [8]–[10] and Sliding Mode Control (SMC) [11]–[17], the literature is quickly developing in the past decade. However, some gaps are still to be filled, specially when Hybrid Electric Vehicles (HEV) are considered, where torque allocation strategies are commonly focused on energy management [1], [2], [18], [19] instead of handling and stability and comprehensive comparative studies are limited.

This paper proposes a case study where a typical segment A passenger vehicle with ICE in Front Wheel Drive (FWD) configuration has two in-wheel EM added in the rear axle to achieve an All-Wheel Drive (AWD) configuration, and these EM are used to perform a DYC strategy.

Two control strategies are compared: a PID controller and a first order SMC. Both prove to be suitable for the established goals. After preliminary results showing issues related to chattering on the SMC control, the influence of hysteresis bands and delays are studied and have only partial influence the vibrational effects.

The system description using a 14 Degrees of Freedom (DoF) model, as well as the control architecture, are described in section II, while in section III the main results are discussed, and the baseline vehicle (AWD without TV) is compared to

the PID controller and to four different configurations of the SMC. The last section displays the main conclusions of this first comparison between controllers for TV in HEV and proposes improvements to the current systems and future developments of the research.

II. Vehicle Modelling and Control Systems

A. Vehicle dynamics and E-Powertrain modelling

To represent the vehicle dynamic response, a 14 DoF model is chosen, namely: 6 DoF for the motion of the vehicle body, 2 DoF per wheel representing their vertical motion and rotation/slip behavior. This modelling approach is well stablished in literature [20], [21] and a synthetic description can be found in [22]. For sake of brevity, the equations of motion shall not be reproduced in this paper. Its implementation using the VI-Grade Car Real Time (CRT) environment allows for a complete representation of each subsystem, as well as a detailed description of the non-linearities encountered in limit adhesion conditions and due to the different powertrain layouts.

The main characteristics of the vehicle based on experimental measurements on a Fiat 500 and literature standard values are displayed in Table I.

TABLE I. VEHICLE MAIN PARAMETERS.

Mass	1006 kg
Wheelbase	2300 mm
Track	1413 mm
CG longitudinal position	805 mm
CG height	537 mm
Tire unloaded radius	291 mm
Tire model	PAC2002_195_65R15
EM peak torque	206 N.m
EM peak power	50 kW

The model includes custom suspension, spring and damper curves, while tire model is based on suitable CRT tires with Pacejka model.

B. E-Powertrain modelling and torque allocation strategy

Simulink environment is used in a co-simulation fashion to model the electric powertrain. Electric motors are represented in a simplified modelling strategy based on the saturation curves of maximum instantaneous power and torque available to an EM that fits the overall dimensions and architecture of in-wheel motors. The battery's model is also simplified and based on a saturation strategy; its characteristics are constant across State of Charge (SOC) levels and do not depend on external factors as temperature.

The Simulink interface is also employed to the control system and torque allocation development. Fig. 2 represents the core control functions and the main blocks (numbered) are described as follows.

Block 1 is responsible for the **Hybrid Logic** of the powertrain, where the repartition between ICE and EM torque is calculated – as a first action, for each timestep the momentaneous EM saturation is calculated based on the EM torque and power maps and the rotational velocity of the wheels. Subsequently a maximum of 50% of the available EM torque is rendered available to be employed to traction purposes. This limitation is chosen to maximize TV possibilities, since it allows a wider range of torque bias without going in saturation.

In this logic, the electric power is preferred over the thermal one, so in low torque request conditions it can be fully satisfied with the EM, while in high torque request conditions the remaining traction is fulfilled by the ICE.

Block 2 is the **Torque Vectoring** block. It is actually a macro structure containing blocks 3-5 that works to decide the allocation of the designated EM total torque between left and right motors.

This logic considers the lateral behavior and actual yaw rate conditions of the vehicle to calculate the necessary yaw moment to reach the desired yaw rate condition, based on the control logic implemented. Further details of each step of such calculation are presented in the description of the single blocks.

Block 3 implements a **Bicycle Model** that computes the *ideal yaw rate* of the vehicle given its longitudinal velocity and the driver's steering input.

The target of this simplified approach is to achieve a balanced lateral behavior throughout all feasible driver requests. The balanced lateral behavior is defined in terms of oversteering or understeering response of the vehicle, knowing that the closer it is to a neutral behavior the higher is the maximum lateral acceleration achievable and the most lateral performance can be obtained.

The 3 DoF model is not able to describe in detail all the complex phenomena related to the single subsystems, to the load transfers or suspension compliance, however, in terms of macroscopic stability and handling response it contains the main factors that influence them [20], [21] with comprehensible parameters and very low computational impact, ideal to control system applications.

To calculate the ideal yaw rate of a balanced vehicle the simplified 3 DoF bicycle model is employed [20], and the understeering coefficient K_u, that determines if the vehicle is under or oversteering, shall be minimized (zero meaning a perfectly neutral response). The ideal yaw rate is defined as the reference for the control system.

Block 4 represents the **Control System** itself.

The controller has as inputs the ideal yaw rate coming from block 3 and the *actual yaw rate* measured at vehicle level through the 14 DoF model, that considers environmental variables, system non-linearities and driver inputs.

Inside this block a switch logic is implemented, in such a way that the user can change from one control strategy to the other, always with the same inputs and outputs.

For both PID and SMC control strategies, the block receives the actual and ideal yaw rates and outputs a control signal proportional to the desired *torque bias*.

Each control system has been individually studied and tunned to achieve good response, by means of their characteristic gains and parameters described in the next section.

Block 5 regards the **Torque Allocation** logic.

It receives the *torque bias* of block 4 signal and translates it in right and left wheel EM torques. It considers the motor saturation for each timestep, avoiding that a too high bias signal creates an exaggerated torque request for the single EM. Also, it must guarantee the desired EM total torque as calculated by block 1. In terms of control hierarchy, the total EM torque has precedence over torque bias, making sure that the total longitudinal torque is always correspondent to the input signal, even if it makes to fall short on the desired bias.
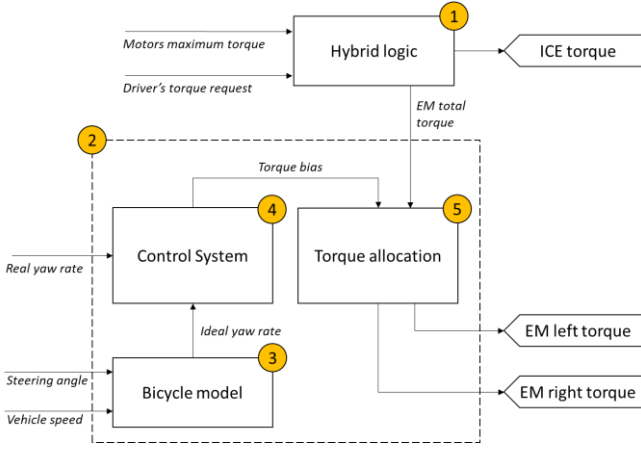
Fig. 2 - Control system and torque allocation scheme as applied in the Simulink model.

Once all torque values are correctly identified, they are feed to the CRT vehicle model each timestep of 0.001 s, capturing all relevant dynamic phenomena.

C. Control systems

Once the vehicle dynamics, electric powertrain and control system are modelled, let us focus on the definition of the control strategies and description of the tested layouts:

The **baseline** HEV (without active TV- denoted '*OFF*' in the plots) is achieved by simply outputting a null control signal, therefore without torque bias.

The **PID** version computes the control signal employing a PID controller as described in (1):

$$K_P(\gamma_i - \gamma_a) + K_I \frac{1}{s}(\gamma_i - \gamma_a) + K_D \frac{F}{1+F\frac{1}{s}}(\gamma_i - \gamma_a) \quad (1)$$

Where: γ_i is the reference ideal yaw rate, γ_a is the actual yaw rate, K_P K_I and K_D are the PID gains, and F is the filtering frequency of the derivative component (values in Table II).

TABLE II.   PID CONTROL GAINS AND FILTER FREQUENCY

K_P	50
K_I	10
K_D	0.01
F	100

Then a first order **SMC** controller is defined as proposed by [23] with the definition of the sliding surface S_1 as in (2):

$$S_1 = (\gamma_i - \gamma_a) \quad (2)$$

Considering the system modelling previously mentioned [20], [21] this sliding surface is known to guarantee stability according to Lyapunov Stability Theory and to achieve the control objective stated as $S_1(t) \to 0$ as $t \to \infty$.

The implementation of the baseline SMC is performed by applying a dedicated function in the Simulink environment based on a symmetric signum function with control action bounded to 100, representing 100% of the available torque of the EM. To fully explore the associated effects and characteristics of the SMC control, two features were included in the analysis: namely a *delay* and a *hysteresis* band. The implemented system allowed the deeper comprehension of these features in overall control

performance and in the chattering, phenomena observed in the first order SMC.

The applied parameters are displayed in Table Table III.

TABLE III.   SMC MAIN PARAMETERS

Control action upper limit	100
Control action lower limit	-100
Hysteresis band	0.4
Delay function Gain	1

The plots in section III display:
- The baseline vehicle without TV (**OFF**)
- The controller based on **PID** strategy
- The baseline **SMC** without delay or hysteresis
- **SMC+delay**
- **SMC+hysteresis**
- **SMC+delay +hysteresis**

D. Maneuver definition

The last step of the modelling phase regards the definition of the maneuver the vehicle is submitted to validate and compare the control strategies. The chosen condition is the Constant Radius Cornering (CRC), where the virtual driver attempt to maintain a fixed path curvature while increasing the longitudinal velocity at a slow rate. This kind of maneuver is commonly used to evaluate quasi-static lateral behavior of vehicles and is suitable for the TV validation since it requires a full range of lateral accelerations and the constant command of throttle to achieve target velocity.

The parameters in Table Table IV are used for the simulations.

TABLE IV.   CONSTANT RADIUS CORNERING PARAMETERS

Initial velocity	30 km/h
Final velocity	108 km/h
Turning radius	80 m
Acceleration start	1 s
Acceleration end	20 s
Total maneuver time	30 s
Transmission gear	Fixed 3rd
Turning direction	Left

The first 1 s of simulation is maintained at constant speed to stabilize the solver. Final target acceleration is set to be higher than 1.1g and fall above the expected adhesion limits of road and tire, thus all configurations shall be saturated and display slipping behavior by the end of the acceleration phase at 20 s. The simulation continues for further 10 s to fully explicit the vehicle's non-linear response.

III. RESULTS

Running all simulation cases with no control system, the PID and the four versions of the SMC strategy, a series of outputs can be obtained ranging from control signal analysis, vehicle state, driver inputs and a detailed graphic interface.

The first step of the post processing is the analysis of the graphic interface, which is useful for results interpretation and quick debugging. In this modality, not easily represented in written form, it is possible to see a pronounced understeering path deviation for the baseline vehicle, while all the controlled versions are much closer and can follow the desired constant radius path for much longer. This is the first

confirmation of the overall better performance of the control systems proposed.

Among the controlled versions the ones with better path following characteristics in the visual inspection are in order: SMC+delay, SMC+delay+hysteresis, SMC, SMC+hysteresis and finally the best performing PID.

Going forward with the plots of key quantities, looking at the left-side EM torque plot in Fig. 3 it is possible to better grasp the real effect of the different control systems.
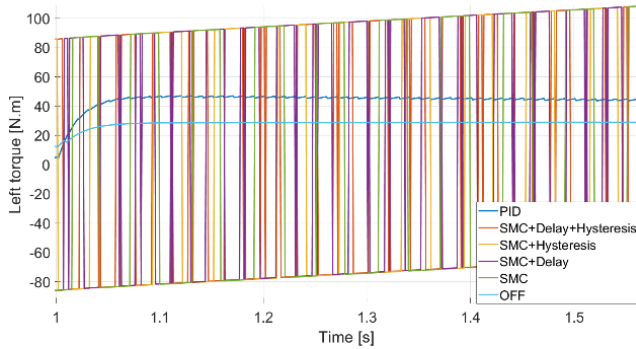

Fig. 3 - Torque in the left-side EM.

The PID controller scales the baseline torque curve to create the and unbalanced torque between sides and generate the desired torque bias. This variation happens in quite smooth and linear manner throughout the whole maneuver, apart from small periodical behavior induced by the derivative part of the PID.

Instead, the SMC system, commanded by a signum function, constantly switches from lower bound saturation to upper bound saturation of the EM based on the status of the yaw rate error. This kind of behavior is expected in first order SMC systems, where the controlled variable is initially taken to the so-called sliding surface (in this case represented by the set of conditions where the vehicle present a neutral lateral response) and then it remains constantly crossing this surface, passing from the slightly understeer to the slightly oversteer behavior. One could think that the control error under such conditions would not be eliminated, since the system continuously goes from one saturated position to the other, but it is the combination of the positions and the frequency and duration of each switch that command the overall average yam moment created. For those familiar with PWM techniques, it is a good link to grasp the working principle.
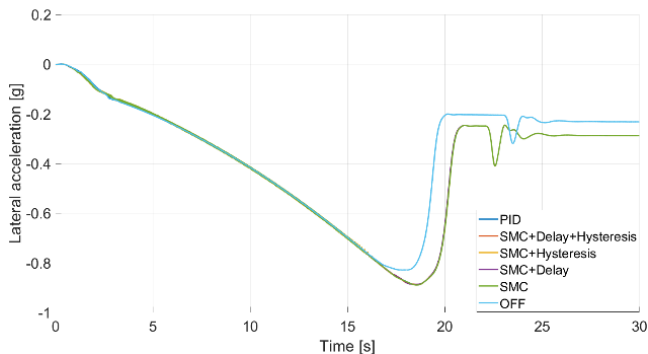

Fig. 4 - Overall lateral acceleration during CRC.

When referring to maximum lateral acceleration, Fig. 4 shows the higher levels achieved by the controlled systems when compared to the baseline. Increments on peak value

between 6,9 and 7,3% are observed, and - although the difference is slim – the best performing strategies are coincident with the best path tracking, as expected.

Looking with more attention the results, one notice that a vibrational behavior emerges.

Fig. 5 shows the a_y curves between 15 and 20 s simulation time and highlights the SMC systems ripple effect throughout the maneuver. The amplitude of the phenomena is consistent at around 0.01 g for SMC and SMC+Hysteresis and 0.0015 g for the versions with the delay feature.

The vibrations cease to exist once the vehicles end their linear zone and start to slip - the reason for that is the response of the control system in saturated condition, where the control signal no longer switches and instead keep the maximum torque bias allowed by the EM.

PID and baseline versions do not display such pattern.
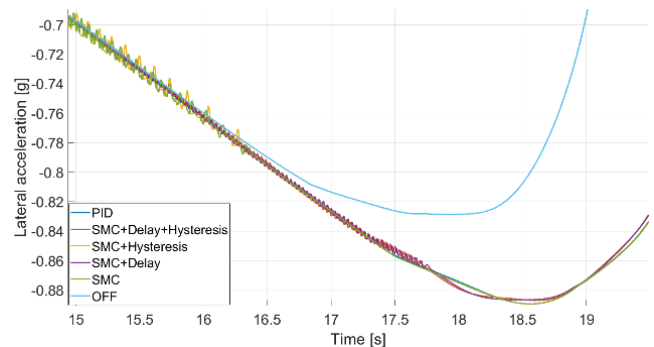

Fig. 5 - Lateral acceleration detail: 15-20 s time range.

Another interesting result can be observed in Fig. 6, where the relation between steering angle and lateral acceleration is analyzed. These curves can be directly related to the goals of DYC displayed in Fig. 1.

All TV systems achieve similar maximum acceleration, while the extension of the linear region is more pronounced for the PID controller and for the SMC without the delay feature. The results are, once again, consistent with the observations of path deviation.

When it comes to the last goal - system responsiveness - it is necessary to zoom in the linear region of the curve (Fig. 7).

All controlled systems improve baseline behavior, and among SMC systems, once again the delay function reduces overall improvement. Comparing the PID and the SMC without the delay feature, it is difficult to establish a clear comparison due to the vibrations, but results suggest similar responsiveness benefits.
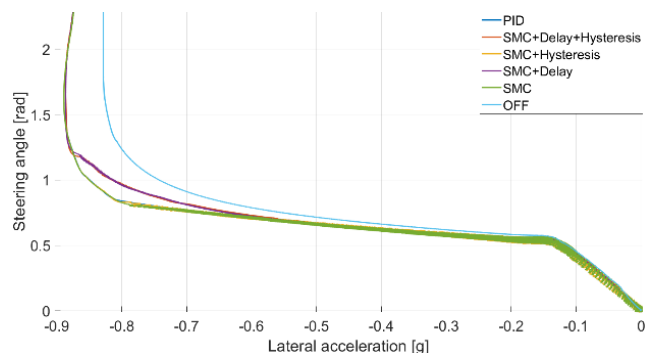

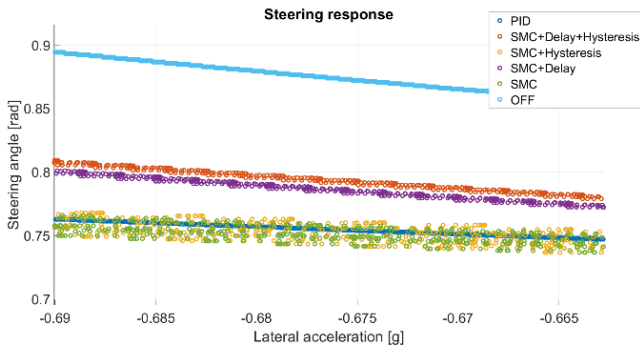Fig. 6 - Steering angle versus Lateral acceleration during CRC.

Fig. 7 - Steering response zoom in the linear region.

Analyzing the yaw rate of the systems, the ripple effect is even more impactful. As shown in Fig. 8 since the very beginning of the CRC the SMC systems display a relevant variation of the yaw rate, particularly for the systems without delay. As noted for the other plots, the vibration stops once the saturation is achieved and the amplitude is consistent during the maneuver. The behavior can be exceptionally troublesome for high-speed straight-line conditions, where minimum steering inputs could trigger exaggerated control responses and threaten overall drivability.
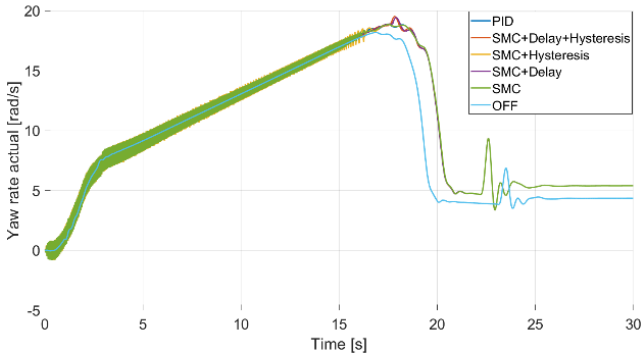

Fig. 8 – Yaw rate evolution during CRC.

It is usual to evaluate control systems by looking at the error they are trying to eliminate. Overall yaw rate error is displayed in Fig. 9 while Fig. 10 shows a detailed focus on the linear region between 3 and 6 s of simulation.
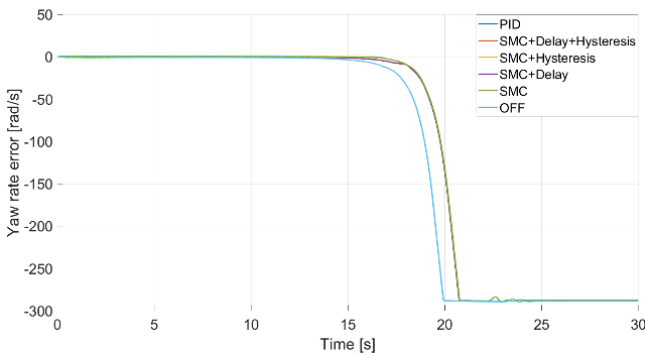

Fig. 9 - Overall yaw rate error during CRC.

Yaw rate error is contained in all cases up to the vicinities of the adhesion limits, and the baseline vehicle is the first to steeply increase the error and detach from target behavior. For the controlled systems, the overall response is comparable, but the focused vision revels an aggressive and unprecise control at lower speeds for the systems with no delay feature. SMC with delay still perform slightly worse than PID and consistently displays low amplitude vibrations, however it remains always below the baseline case, showing a consistent improvement in error elimination.
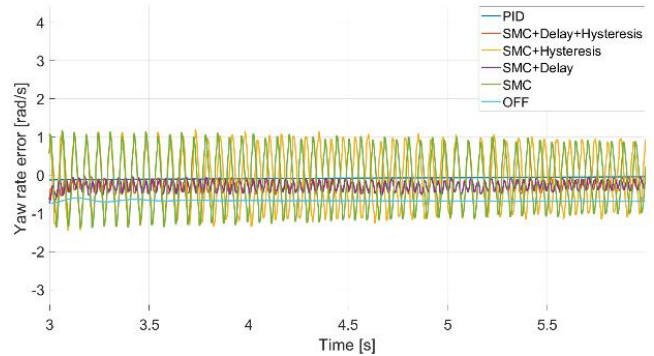

Fig. 10 – Yaw rate error detail: zoom in the linear region.

A final verification is necessary to fully comprehend the results obtained by the simulation: the steering inputs given by the driver during the maneuver (Fig. 11).
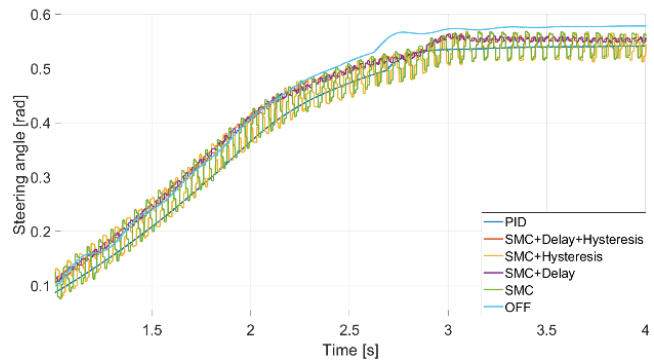

Fig. 11 - Steering angle in the CRC: detail in the 1-4 s range

Since the very beginning of the simulation the virtual driver is required to give constant steering inputs to keep the vehicle close to the desired trajectory. These corrections happen in a very high frequency and with uttermost precision. However, due to the nature of the system, the steering angle is a parameter used in the ideal yaw rate computation, so that it is tricky to state its net impact on the vibrational behavior.

Previous works highlight the importance of Driver in the Loop validations for control systems [6], [24], [25] – using prototypes or driving simulators – to guarantee that the strategy is user friendly. Further investigations shall be performed to evaluate how a human driver would respond to a SMC system as proposed in terms of driving precision and perceived comfort.

IV. CONCLUSION

This paper represents a first step on the comprehensive study of TV control systems for HEV. Particularly a comparison between PID and SMC strategies for TV in a HEV with rear in-wheel motors is presented. Both control architectures are suitable for achieving the DYC goals of increase lateral acceleration, extending steering linear region and improving vehicle responsiveness.

Overall lateral performance is considered similar among controlled systems; however, the SMC presents a tendency to

induce vibrational behavior in the vehicle and trigger potential comfort and handling problems.

The chattering behavior is observed in all the SMC systems, with or without the presence of the delay and hysteresis features. The delayed control system showed a smaller amplitude on the vibrations together with a reduction on the path following precision near limit conditions. The presence of a hysteresis band had little effect in all cases.

Further investigation will be focused on: the implementation of chattering reduction strategies [26], [27] second-order SMC [28], [29] and Simplex algorithms [30], [31]; Implementation and experimental validation of the obtained results; and Inclusion of other control strategies, such as MPC and Linear Quadratic.

REFERENCES

[1] M. Carello, P. Bonansea, and M. D'Auria, "Driveline Optimization for a Hybrid Electric City Vehicle to Minimize Fuel Consumption," in *SAE 2014 World Congress & Exhibition*, Apr. 2014, pp. 2014-01-1090, doi: 10.4271/2014-01-1090.

[2] C. Cubito, L. Rolando, A. Ferraris, M. Carello, and F. Millo, "Design of the control strategy for a range extended hybrid vehicle by means of dynamic programming optimization," in *2017 IEEE Intelligent Vehicles Symposium (IV)*, Redondo Beach, CA, USA, Jun. 2017, pp. 1234–1241, doi: 10.1109/IVS.2017.7995881.

[3] H. de Carvalho Pinheiro *et al.*, "Dynamic Performance Comparison Between In-Wheel and On-Board Motor Battery Electric Vehicles," presented at the ASME 2020 International Design Engineering Technical Conferences and Computers and Information in Engineering Conference, Nov. 2020, doi: 10.1115/DETC2020-22306.

[4] H. de Carvalho Pinheiro, A. Messana, L. Sisca, A. Ferraris, A. G. Airale, and M. Carello, "Torque Vectoring in Electric Vehicles with In-wheel Motors," in *Advances in Mechanism and Machine Science*, 2019, pp. 3127–3136, doi: 10.1007/978-3-030-20131-9_308.

[5] H. de Carvalho Pinheiro *et al.*, "All-wheel drive electric vehicle modeling and performance optimization," presented at the SAE Brasil 2019, 2019, doi: https://doi.org/10.4271/2019-36-0197.

[6] A. Ferraris, H. de Carvalho Pinheiro, E. Galanzino, A. G. Airale, and M. Carello, "All-Wheel Drive Electric Vehicle Performance Optimization: From Modelling to Subjective Evaluation on a Static Simulator," EV 2019 Electric Vehicles International Conference, 2019, doi: 10.1109/EV.2019.8893027.

[7] F. Assadian and M. Hancock, "A comparison of yaw stability control strategies for the active differential," in *Proceedings of the IEEE International Symposium on Industrial Electronics, 2005. ISIE 2005.*, Jun. 2005, vol. 1, pp. 373–378, doi: 10.1109/ISIE.2005.1528939.

[8] E. Siampis, E. Velenis, and S. Longo, "Predictive rear wheel torque vectoring control with terminal understeer mitigation using nonlinear estimation," in *2015 54th IEEE Conference on Decision and Control (CDC)*, Dec. 2015, pp. 4302–4307, doi: 10.1109/CDC.2015.7402890.

[9] E. Siampis, E. Velenis, and S. Longo, "Model Predictive torque vectoring control for electric vehicles near the limits of handling," in *2015 European Control Conference (ECC)*, Jul. 2015, pp. 2553–2558, doi: 10.1109/ECC.2015.7330922.

[10] "An Energy-Saving Torque Vectoring Control Strategy for Electric Vehicles Considering Handling Stability Under Extreme Conditions," *IEEE Trans. Veh. Technol.*, vol. 69, no. 10, pp. 10787–10796, doi: 10.1109/TVT.2020.3011921.

[11] T. Goggia, A. Sorniotti, L. De Novellis, and A. Ferrara, "Torque-vectoring control in fully electric vehicles via integral sliding modes," in *2014 American Control Conference*, Jun. 2014, pp. 3918–3923, doi: 10.1109/ACC.2014.6858807.

[12] M. Canale, L. Fagiano, A. Ferrara, and C. Vecchio, "Vehicle Yaw Control via Second-Order Sliding-Mode Technique," *IEEE Trans.*

Ind. Electron., vol. 55, no. 11, pp. 3908–3916, Nov. 2008, doi: 10.1109/TIE.2008.2003200.

[13] Z. Wang, Y. Wang, L. Zhang, and M. Liu, "Vehicle Stability Enhancement through Hierarchical Control for a Four-Wheel-Independently-Actuated Electric Vehicle," *Energies*, vol. 10, no. 7, Art. no. 7, Jul. 2017, doi: 10.3390/en10070947.

[14] X. Xu, L. Xiong, and Y. Feng, "Torque Vectoring Control for Handling Improvement of 4WD EV," *Adv. Mater. Res.*, vol. 765–767, pp. 1893–1898, 2013, doi: 10.4028/www.scientific.net/AMR.765-767.1893.

[15] M. Chae, Y. Hyun, K. Yi, and K. Nam, "Dynamic Handling Characteristics Control of an in-Wheel-Motor Driven Electric Vehicle Based on Multiple Sliding Mode Control Approach," *IEEE Access*, vol. 7, pp. 132448–132458, 2019, doi: 10.1109/ACCESS.2019.2940434.

[16] A. Tota *et al.*, "On the Experimental Analysis of Integral Sliding Modes for Yaw Rate and Sideslip Control of an Electric Vehicle with Multiple Motors | SpringerLink," *Int. J. Automot. Technol.*, vol. 19, pp. 811–823, 2018, doi: 10.1007/s12239-018-0078-0.

[17] J. Zehetner and M. Horn, "Vehicle dynamics control with torque vectoring and active rear steering using sliding mode control," *IFAC Proc. Vol.*, vol. 40, no. 10, pp. 1–8, Jan. 2007, doi: 10.3182/20070820-3-US-2918.00003.

[18] M. Carello, H. de Carvalho Pinheiro, L. Longega, and L. Di Napoli, "Design and Modelling of the Powertrain of a Hybrid Fuel Cell Electric Vehicle," presented at the SAE WCX Digital Summit, Apr. 2021, doi: 10.4271/2021-01-0734.

[19] M. Carello, N. Filippo, and R. d'Ippolito, "Performance Optimization for the XAM Hybrid Electric Vehicle Prototype," in *SAE 2012 World Congress & Exhibition*, Apr. 2012, pp. 2012-01–0773, doi: 10.4271/2012-01-0773.

[20] W. F. Milliken, *Race Car Vehicle Dynamics*. Society of Automotive Engineers, 1995.

[21] G. Genta and L. Morello, *The Automotive Chassis: Volume 1-2*. Springer Science & Business Media, 2008.

[22] J. D. Setiawan, M. Safarudin and A. Singh, "Modeling, simulation and validation of 14 DOF full vehicle model," *International Conference on Instrumentation, Communication, Information Technology, and Biomedical Engineering,* 2009, pp. 1-6, doi: 10.1109/ICICI-BME.2009.5417285.

[23] V. I. Utkin, *Sliding Modes in Control and Optimization*. Berlin Heidelberg: Springer-Verlag, 1992.

[24] H. de Carvalho Pinheiro *et al.*, "Active Aerodynamics Through Active Body Control: Modelling and Static Simulator Validation," presented at the ASME 2020 International Design Engineering Technical Conferences and Computers and Information in Engineering Conference, Nov. 2020, doi: 10.1115/DETC2020-22298.

[25] H. de Carvalho Pinheiro *et al.*, "Advanced Vehicle Dynamics Through Active Aerodynamics and Active Body Control," presented at the ASME 2020 International Design Engineering Technical Conferences and Computers and Information in Engineering Conference, Nov. 2020, doi: 10.1115/DETC2020-22290.

[26] G Bartolini, E Punta, T Zolezzi, "Simplex sliding mode control of multi-input systems with chattering reduction and mono-directional actuators," *Automatica* 47 (11), 2433-2437, 2011, doi: 10.1016/j.automatica.2011.08.011.

[27] G Bartolini, E Punta, "Multi-input sliding mode control of nonlinear uncertain non-affine systems with mono-directional actuation," *IEEE Transactions on Automatic Control* 60 (2), 393-403, 2015, doi: 10.3182/20130204-3-FR-2033.00161.

[28] A Levant, "Sliding order and sliding accuracy in sliding mode control," *International journal of control* 58 (6), 1247-1263, 1993, doi: 10.1080/00207179308923053.

[29] M Canale, L Fagiano, A Ferrara, C Vecchio, "Comparing internal model control and sliding-mode approaches for vehicle yaw control," *IEEE Transactions on Intelligent Transportation Systems* 10 (1), 31-41, 2008, doi: 10.1109/TITS.2008.2006772.

[30] S. V. Bajda and D. B. Izosimov, "Vector method of design of sliding motion and simplex algorithms," *Automat. Remote Control*, vol. 46, pp. 830–837, 1985

[31] G Bartolini, E Punta, T Zolezzi, "Simplex methods for nonlinear uncertain sliding-mode control," *IEEE Transactions on Automatic Control* 49 (6), 922-933, 2004, doi: 10.1109/TAC.2004.829617.